Biosensors and Bioelectronics 291 (2026) 118051

Contents lists available at ScienceDirect

Biosensors and Bioelectronics

journal homepage: www.elsevier.com/locate/bios

Deep learning-driven morphological analysis for assessing EMT state and drug sensitivity of single tumor cell

Yiyao Yang [a,1], Yuxin Guo [b,1], Zhaoliang Wang [c], Yifan Weng [d], Tingting Hao [a], Qingqing Zhang [a], Shuihua Wang [b,*], Zhiyong Guo [a,**]

[a] State Key Laboratory for Quality and Safety of Agro-Products, School of Materials Science and Chemical Engineering, Ningbo University, Ningbo, 315211, PR China
[b] Department of Biological Sciences, Xi'an Jiaotong-Liverpool University, Suzhou, 215123, PR China
[c] Library, Ningbo University of Technology, Ningbo, 315211, PR China
[d] Xiangya School of Medicine, Central South University, Changsha, 410013, PR China

ARTICLE INFO

Keywords:
Deep learning
Morphological analysis
Circulating tumor cells (CTCs)
Epithelial-mesenchymal transition (EMT)
Drug sensitivity
Single tumor cell

ABSTRACT

Metastasis driven by the epithelial-mesenchymal transition (EMT) in circulating tumor cells (CTCs) is a major challenge in cancer treatment. Current EMT assessment methods rely on invasive detection of protein or genetic markers, lack single-cell resolution, and fail to provide real-time dynamic insights, especially for rare CTCs. Here, we developed a convolutional neural network (CNN)-based deep learning model that quantifies EMT states in single or scarce CTCs through non-invasive, label-free morphological profiling. First, TGF-β-stimulated EMT induction in MCF-7 cells was monitored through quantitative assessment of EMT-related protein expression, identifying key transitional timepoints. Then, five distinct morphological states representing EMT progression were selected via combined morphological observation. Finally, cellular images from these states were processed by the developed convolutional neural network (CNN) model, which performs label-free morphological profiling at single-cell resolution. This approach enables real-time, individualized evaluation of metastatic potential, advancing precision diagnostics and therapeutic strategies for cancer management.

1. Introduction

Metastasis remains a major obstacle to successful cancer treatment and the leading cause of cancer-related mortality (Kiri and Ryba, 2024; Castaneda et al., 2022; Ganesh and Massague, 2021; Mani et al., 2024; Qian et al., 2017). The epithelial-mesenchymal transition (EMT) in tumor cells significantly enhances their invasive and metastatic potential by suppressing epithelial phenotypic markers while activating mesenchymal characteristic genes. Therefore, the EMT-associated state alteration demonstrates substantial clinical relevance in cancer management (Christiansen and Rajasekaran, 2006; Gerashchenko et al., 2016; Jinesh and Brohl, 2022; Khanbabaei et al., 2022; Lo and Zhang, 2018; Pang et al., 2018; Pastushenko and Blanpain, 2019; Saitoh, 2023; Simeonov et al., 2021; Singh et al., 2018).

Current mainstream approaches for assessing EMT state primarily rely on detection of EMT-related proteins (e.g., N-cadherin, E-cadherin, Vimentin, Occludin) and transcription factors (e.g., Snail, Twist, Zeb 1). However, these methods typically require cell lysis, labeling, or staining procedures, which inevitably result in cellular damage and make it difficult to obtain real-time, dynamic information on EMT state (Erin et al., 2020; Fang and Kang, 2021; Li et al. 2017, 2021; Puchinskaya, 2019; Puchinskaya and Prokopenia, 2020; Serrano-Gomez et al., 2016; Ulianova et al., 2021; Yang et al., 2016; Zhang and Stuelten, 2024). Furthermore, population-level detection strategies obscure the critical impact of single-cell heterogeneity on metastatic processes (Diamantopoulou et al., 2020; Kitz et al., 2021). Additionally, the technical challenge is compounded by the extreme scarcity of circulating tumor cells (CTCs), which are the actual metastatic precursors in clinical specimens, making their EMT state particularly difficult to characterize. Consequently, developing methodologies for individualized assessment of EMT state in single or rare CTCs holds significant implications for analyzing anticancer drug sensitivity, monitoring metastatic progression, and formulating personalized therapeutic strategies.

Although morphological alterations during EMT enable preliminary

* Corresponding author.
** Corresponding author.
E-mail addresses: Shuihua.Wang@xjtlu.edu.cn (S. Wang), guozhiyong@nbu.edu.cn (Z. Guo).
[1] Yiyao Yang and Yuxin Guo contributed equally to this work.

https://doi.org/10.1016/j.bios.2025.118051
Received 18 July 2025; Received in revised form 27 September 2025; Accepted 28 September 2025
Available online 29 September 2025
0956-5663/© 2025 Elsevier B.V. All rights are reserved, including those for text and data mining, AI training, and similar technologies.

assessment of cellular states, conventional evaluations suffer from substantial subjective variability and lack standardized quantitative metrics (Ida et al., 2025; Nakaya and Sheng, 2013; Nurmagambetova et al., 2023; Quinsgaard et al., 2024; Savagner, 2010; Zhao et al., 2021). Deep learning techniques, leveraging their powerful image feature extraction capabilities, have demonstrated remarkable advantages in overcoming human interpretation biases and have been widely implemented in tumor cell classification (Calderaro et al., 2023; Courtiol et al., 2019; Gao et al., 2022; Li, 2023; Moen et al., 2019; Vermeulen et al., 2023; Whitney et al., 2020), recognition, segmentation, prediction and screening (Balagopal et al., 2021; Ertl-Wagner and Khalvati, 2021; Gagnon et al., 2023; Jiang et al., 2023; Lee and Jang, 2022; Sandino et al., 2021; Tian et al., 2024; Wu et al., 2020; Zeune et al., 2020). However, no existing deep learning-based methodology has been reported for individualized EMT state evaluation in single or limited CTCs.

This study innovatively developed a convolutional neural network-based deep learning model that enables real-time dynamic quantification of EMT state in CTCs through single-cell morphological profiling, thereby advancing precision oncology applications.

2. Materials and methods

Materials and reagents, instruments and cell culture are shown in Supporting Information.

2.1. Image data collection and preprocessing

Epithelial-mesenchymal transition (EMT) of MCF-7 cells was induced by transforming growth factor-β1 (TGF-β1) as follows: (1) The above culture dishes were maintained in 5 % CO_2 at 37 °C for 12 h to ensure well adhesion. The spent medium was discarded, and adherent cells were gently rinsed with 1 mL of 1 × PBS, followed by replenishment with 1 mL of fresh culture medium. (2) After 1 min, 250 μL 5 ng/mL TGF-β1 solution was added and then 50 μL of 5 ng/mL TGF-β1 was added at 1, 2, 3, and 4 h. Images of cells in states i, ii, iii, iv, and v were taken at 0, 1.5, 2.5, 3.5, and 4.5 h, respectively, with cells maintained under standard culture conditions except during imaging sessions. (3) A total of 1516 cell images across five EMT states were obtained. Individual cell morphologies were delineated using the Cellpose segmentation tool, followed by label-specific processing for single-cell analysis.

2.2. Construction of the deep learning model

The preprocessed images were organized into a state-labeled dataset, which was randomly partitioned into training, validation, and test sets at a ratio of 6 : 3: 1.

To enhance model generalizability, multimodal data augmentation strategies was implemented to strengthen feature recognition capabilities. The following methods are included: (1) Illumination augmentation: RandomBrightnessContrast and HueSaturationValue were applied to compensate for microscope light source fluctuations and imaging variability, improving robustness against illumination changes. (2) Channel randomization: Channel shuffling disrupted model dependency on fixed RGB channel orders, reinforcing spatial feature learning. (3) Geometric transformations: Horizontal/vertical flipping and random rotation simulated stochastic cellular growth orientations in culture systems while preserving morphological topology. (4) Deformation modeling: Thin Plate Spline interpolation emulated nonlinear optical distortions in microscope imaging, enhancing adaptability to elastic cellular deformations. (5) Affine transformation: Linear spatial variations (translation, scaling, shear) generated via affine operations mimicked stage displacement artifacts while maintaining structural consistency.

The augmented images were fed into the YOLOv11 architecture for training cellular invasion capability assessment. The model workflow comprised three stages: (1) Feature extraction: Multi-scale semantic features were hierarchically extracted from input images. (2) Feature fusion: Cross-scale information flow was optimized through integration of heterogeneous feature layers. (3) Classification detection: Parallel predictions on multi-scale feature maps yielded target localization, class probabilities, and confidence scores, ultimately outputting single-cell-level invasion capability assessments.

2.3. ELISA assay

The steps were as follows: (1) The cell suspension was transferred to 2 mL centrifuge tubes and centrifuged at 1000×*g* for 10 min to collect the supernatant. (2) Standard wells: 50 μL of serially diluted standards (S0-S5: 0, 0.5, 1, 2, 4, 8 ng/mL) was added to designated wells. Sample wells: 10 μL of supernatant mixed with 40 μL of sample dilution buffer was loaded. Blank wells: No reagents were added. (3) Horseradish peroxidase (HRP)-conjugated detection antibody (100 μL/well) was added to all wells except blank wells. Plates were sealed with adhesive film and incubated at 37 °C for 60 min (4) Liquid was discarded, and wells were blotted dry on absorbent paper. Each well was filled with diluted wash buffer, incubated for 1 min, then emptied. This washing cycle was repeated five times. (5) 50 μL of substrate A and B was added to each well, respectively, followed by 15 min dark incubation at 37 °C. (6) 50 μL of stop solution was added per well. The absorbance at 450 nm was measured within 15 min by Infinite M200 PRO, and a standard curve was constructed for quantitative analysis.

2.4. Collection of clinical samples

Peripheral blood samples were collected from healthy adult volunteers using EDTA vacuum tubes. Collected blood samples were processed within 2 h of collection. All experiments involving spiked-in MCF-7 cells were performed on the same day the blood was drawn. Cellular images were acquired under standardized conditions and analyzed using the developed deep learning model to assess invasive capability. This study was approved by the Ethics Committee of Ningbo University (Approval No.: NBU-W-2022-001), and all experiments were conducted with full informed consent from participants.

2.5. Protocol of assessing drug sensitivity

(1) Cell preparation: MCF-7 cells at state V were selected, and residual TGF-β1 growth factor was aspirated from culture dishes. A matrix replacement was performed using DMEM basal medium, with 1 mL of fresh DMEM added per dish to establish a standardized drug-response microenvironment. (2) Drug intervention: Four chemotherapeutic agents were prepared as working solutions (calibrated to 10 mM): Platinum-based agent: Cisplatin; Microtubule stabilizer: Paclitaxel; Topoisomerase inhibitor: Doxorubicin; mTOR inhibitor: Rapamycin. Equal volumes (50 μL) of drug solutions were added to designated culture dishes via parallel pipetting to achieve target final concentrations, respectively. Post-administration, dishes were incubated at room temperature for 10 min to ensure complete drug diffusion across the cellular monolayer. (3) Microscopic imaging: Time-lapse imaging was conducted by CKX53 inverted microscope to capture early-stage morphological alterations induced by drug exposure.

This experimental protocol ensures comparability across drug treatment groups through standardized drug concentrations, controlled incubation durations, and normalized imaging parameters. The 10 mM drug concentration was established based on preliminary dose-response optimization studies, which demonstrated its capacity to reliably induce observable morphological alterations in cells while maintaining experimental reproducibility under defined operational conditions.

3. Results and discussion

3.1. Principle of deep learning-based EMT state and drug sensitivity profiling in CTCs

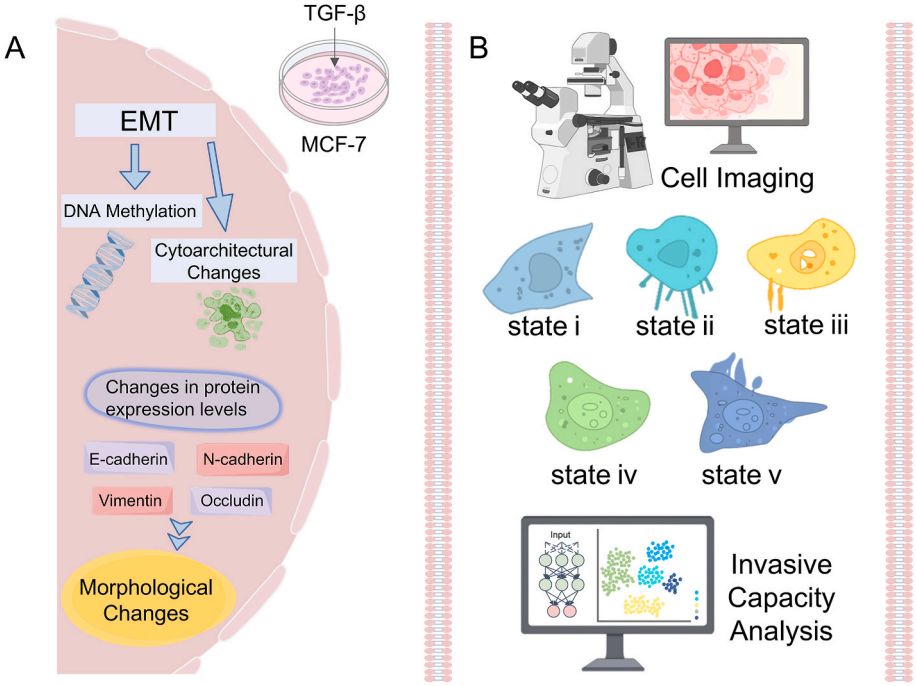
Scheme 1 illustrates a deep learning-driven morphological analysis framework for evaluating epithelial-mesenchymal transition (EMT) states and drug sensitivity in single circulating tumor cells (CTCs). Initially, TGF-β-stimulated EMT induction in MCF-7 cells was monitored through quantitative assessment of EMT-related protein expression, identifying key transitional timepoints. Five distinct morphological states representing EMT progression were selected via combined morphological observation. Cellular images from these states were processed by a convolutional neural network (CNN) model, which performs label-free morphological profiling at single-cell resolution. The model dynamically classifies EMT states and quantifies metastatic potential (invasion capacity), thereby enabling individualized drug sensitivity analysis for precision oncology applications.

3.2. Feasibility of assessing EMT state via cellular morphology

Expression of key proteins during TGF-β1-induced epithelial-mesenchymal transition (EMT), enzyme-linked immunosorbent assay (ELISA) was performed to quantify changes in N-cadherin, E-cadherin, Vimentin, and Occludin levels in MCF-7 cells exposed to TGF-β1 for varying durations (0, 1.5, 2.5, 3.5, and 4.5 h), as shown in Fig. 1A–D. During the initial four time points (0–3.5 h), E-cadherin expression was progressively downregulated, while N-cadherin exhibited significant upregulation, demonstrating the characteristic "E/N-cadherin switch" that reflects core molecular events of EMT progression. Specifically, the replacement of E-cadherin by N-cadherin in epithelial cells reduces intercellular adhesion strength and enhances migratory and invasive capabilities. Concurrently, Vimentin levels continuously increased during this phase. As an intermediate filament protein, Vimentin facilitates cytoskeletal remodeling, endowing cells with enhanced mechanical stability and motility. In contrast, Occludin expression declined, leading to loosened intercellular tight junctions and further promoting the transition toward a mesenchymal phenotype. However, at 4.5 h post-treatment, partial recovery of expression levels was observed for all four proteins. This phenomenon may stem from negative feedback regulation triggered by sustained TGF-β1 stimulation through activation of non-canonical signaling pathways, or partial reversion to epithelial characteristics mediated by synergistic microenvironmental factors. Notably, given the irreversible nature of epigenetic reprogramming during EMT, complete restoration of the original epithelial phenotype remains unlikely. Complementary morphological observations (Fig. 1E–I) revealed state-dependent phenotypic transitions: State i: displayed typical epithelial morphology with regular polygonal shapes and dense intercellular junctions (Fig. 1E); State ii: exhibited cytoskeletal remodeling with spindle-like protrusions while maintaining cellular connections (Fig. 1F); State iii: demonstrated elongated cell bodies, reduced contact areas, and enhanced filopodia formation (Fig. 1G); State iv: showed free-floating cells with rounded morphology and diminished polarity, indicative of advanced mesenchymal transition (Fig. 1H); State v: presented a metastable epithelial-like morphology with blurred organelle contours and reduced metabolic activity (Fig. 1I). These morphological alterations align temporally with the protein expression patterns, establishing cell shape characteristics as reliable indicators for EMT status assessment and potential invasiveness prediction, thereby providing morphological criteria for phenotypic evaluation during EMT processes.

3.3. Performance of deep learning model for morphological analysis

The effects of data augmentation applied to training set images are illustrated in Supplementary Fig. S1. Enhanced statistical analysis in Fig. S2 demonstrates a balanced data distribution across categories with minimal inter-state dataset disparities and appropriate bounding box dimensions, indicating robust generalization capability and stability of the model. Upon feeding cell images of distinct phenotypic states into the constructed deep learning model, the output results (Fig. 2A–E) reveal precise classification of circulating tumor cells (CTCs) into corresponding epithelial-mesenchymal transition (EMT) states, coupled with quantitative assessment of invasive potential variations among CTCs within the same EMT state. For instance, state i classifications are marked with blue borders accompanied by quantified matching scores



Scheme 1. Schematic diagram of deep learning-driven morphological analysis for assessing EMT state and drug sensitivity of single tumor cell.

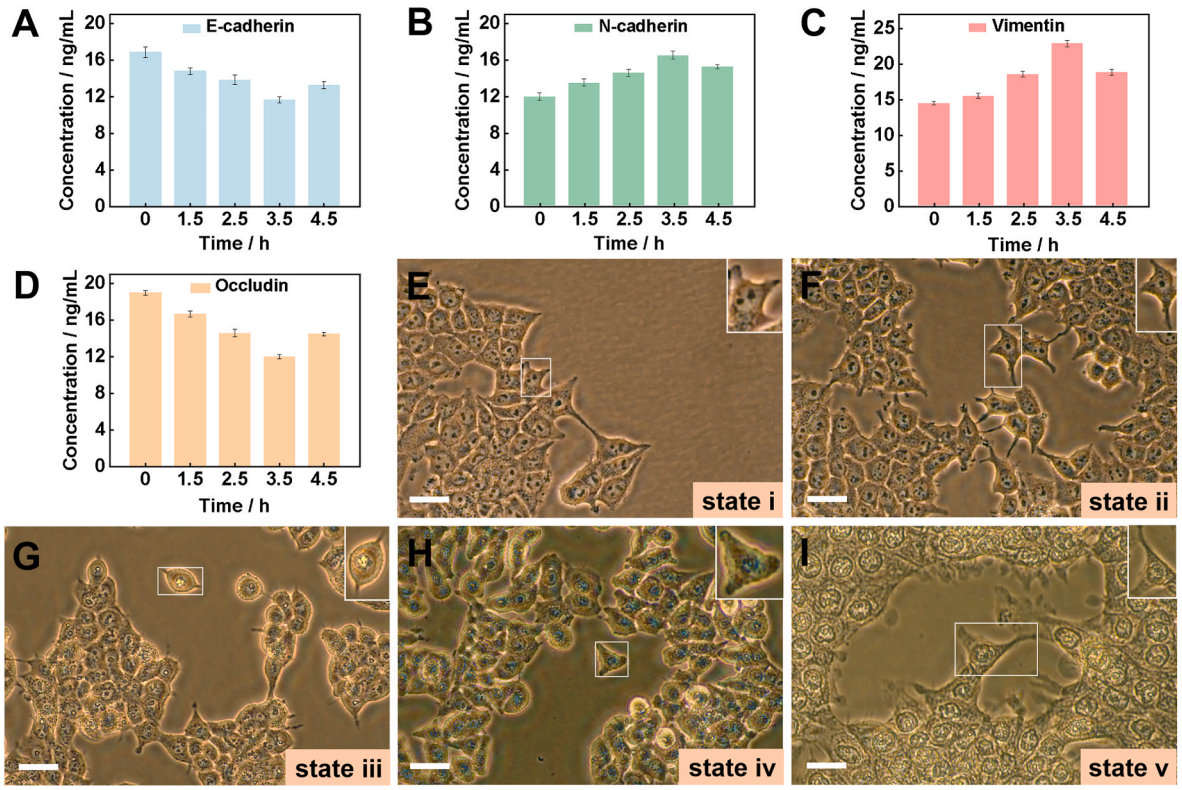


Fig. 1. Changes in protein expression levels of E-cadherin, N-cadherin, Vimentin, and Occludin during EMT: (A) E-cadherin, (B) N-cadherin, (C) Vimentin, and (D) Occludin. Cell images of five states: (E) state i, (F) state ii, (G) state iii, (H) state iv, and (I) state v. Scale bar, 10 μm.

between individual cells and state i reference features, while states ii-v are differentiated through cyan, white, green, and navy-blue identifiers. This dual-output architecture enables simultaneous EMT state classification and parametric invasion capability analysis. The confusion matrix (Fig. 2F) confirms high prediction accuracy across all five cellular states. Subsequent evaluation using standard YOLO model metrics (Fig. 2G) demonstrates superior performance under biologically challenging conditions. Despite significant morphological heterogeneity and classification complexity, the model achieves mAP 50 values exceeding 95 % after 60 epochs, reflecting robust performance across varying IoU thresholds. The precision and recall metrics gradually stabilized during later training phases, indicating that the model achieved a correct prediction and classification rate exceeding 96 % for cellular states, with high coincidence rate between the actual bounding boxes and the predicted bounding boxes indicates favorable prediction accuracy.

Comparative analysis with classical YOLO architectures (YOLOv5, YOLOv6, and YOLOv8) highlights the superiority of our model's optimized feature extraction mechanism in capturing critical cellular state information, delivering state-of-the-art object detection accuracy (Fig. S3, Table S1). Moreover, model validation results (Fig. S4) demonstrate that all performance metrics reach advanced levels, with the F1 score approaching the theoretical maximum, indicating an optimal balance between precision and recall. Confidence threshold analysis reveals positive correlation between precision and threshold elevation, achieving 100 % accuracy at a threshold of 0.897. In multi-class detection tasks, precision curves for all five target categories maintain stable upward trajectories, while recall curves exhibit expected inverse relationships with threshold increments, aligning with fundamental target detection principles. PR curve analysis further validates model robustness, showing minimal precision fluctuations during recall enhancement while maintaining high-level stability. These characteristics confirm the classifier's exceptional discriminative capacity across samples of varying detection complexities, substantiating its practical value in sophisticated biomedical image analysis. Collectively, the YOLOv11 model demonstrates superior performance in single-CTC EMT state analysis and invasion potential quantification, outperforming comparable architectures in cellular feature interpretation and image-based predictive analytics.

3.4. Assessing EMT state of CTC in whole blood

Cellular images from whole blood samples were processed through the constructed deep learning model for invasive capacity analysis of CTCs, with results displayed in Fig. 3A–F. The model demonstrated efficient and accurate identification of CTCs within complex hematological backgrounds, while simultaneously determining their EMT states and invasive capacities based on cellular morphological characteristics.

3.5. Assessing drug sensitivity of CTC

MCF-7 cells stimulated to state v by TGF-β1 were treated with four drugs, and the acquired cellular images were processed through the constructed deep learning model. Drug efficacy results for cisplatin (Fig. 4A), paclitaxel (Fig. 4B), doxorubicin (Fig. 4C), and rapamycin (Fig. 4D) are illustrated. Paclitaxel (Fig. 4B) demonstrated the highest efficacy in reversing EMT, with treated cells predominantly exhibiting EMT-reversed phenotypes (states i, ii, and iii) and the highest proportion of epithelial-state cells, characterized by reconstructed polarity and regenerated intercellular junctions. In contrast, rapamycin (Fig. 4D) shows minimal EMT reversal, as most cells remain in state iv with sustained mesenchymal characteristics. These findings validate the validity and applicability of the deep learning model for multi-drug screening and cellular drug sensitivity evaluation.

3.6. Comprehensive discussion

In this study, we established a deep learning-driven framework for non-invasive, label-free morphological profiling to quantify EMT states

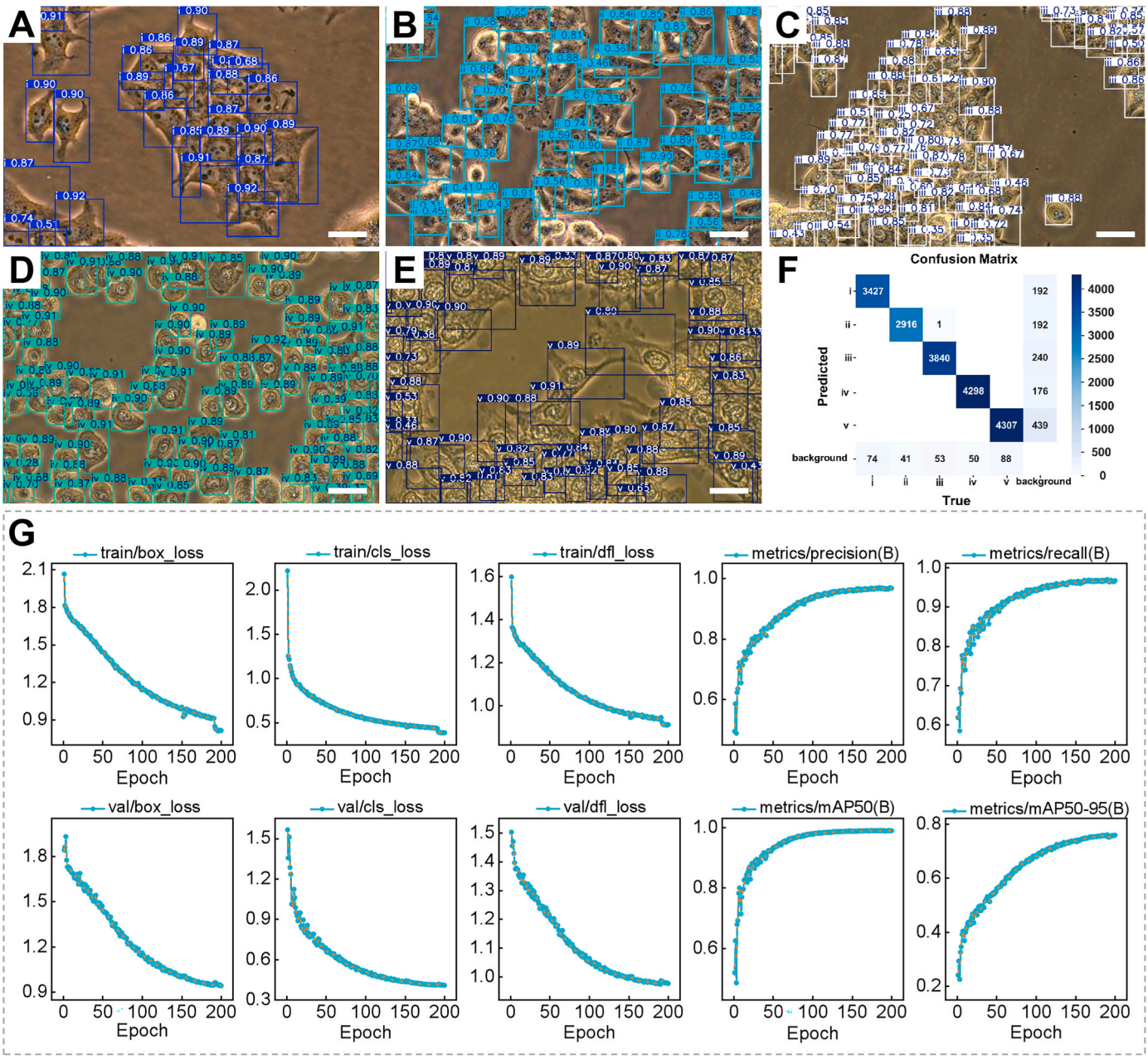


Fig. 2. Deep learning model analysis of EMT states in five states: (A) state i, (B) state ii, (C) state iii, (D) state iv, and (E) state v. (F) Confusion matrix. (G) Model performance metrics: Training-phase bounding box, classification, and dynamic feature losses; precision; recall; validation-phase bounding box, classification, and dynamic feature losses; average precision; mean average precision. Scale bar: 10 μm.

and predict drug sensitivity at single-cell resolution. The principal innovation of our work lies in its capacity to dynamically assess EMT progression without the need for biomarkers and to successfully analyze rare CTCs within the complex background of whole blood.

Traditional techniques for evaluating EMT, such as immunofluorescence, Western blot, and qPCR, rely on the detection of biomolecular markers. Although these methods provide molecular-level information, they require cell fixation, lysis, or labeling, which prevent real-time dynamic monitoring and non-invasive analysis. In contrast, our approach enables continuous monitoring of the EMT process while preserving cell viability, offering a novel technical platform for investigating dynamic EMT transitions.

Existing morphological analysis based on computer vision often relied on hand-crafted features, which were limited in expressiveness and generalizability. Although deep learning has been increasingly applied to cell classification and segmentation, most studies have focused on cell type identification or basic morphological parameter measurement. To our knowledge, this is the first study to employ the YOLOv11 architecture for simultaneous EMT state classification and invasion capability assessment, providing interpretable outputs with high accuracy at single-cell resolution. In addition, compared with cell segmentation methods based on U-Net or Mask R-CNN, our approach not only achieves cell segmentation but also accomplishes EMT state classification and quantitative invasion assessment, delivering more comprehensive functionality. Furthermore, relative to traditional classification networks such as ResNet or Vision Transformer, YOLOv11 maintains high accuracy while offering superior real-time performance and multi-scale detection capabilities, making it more suitable for clinical translation.

The core advantages of our method are threefold: First, it enables

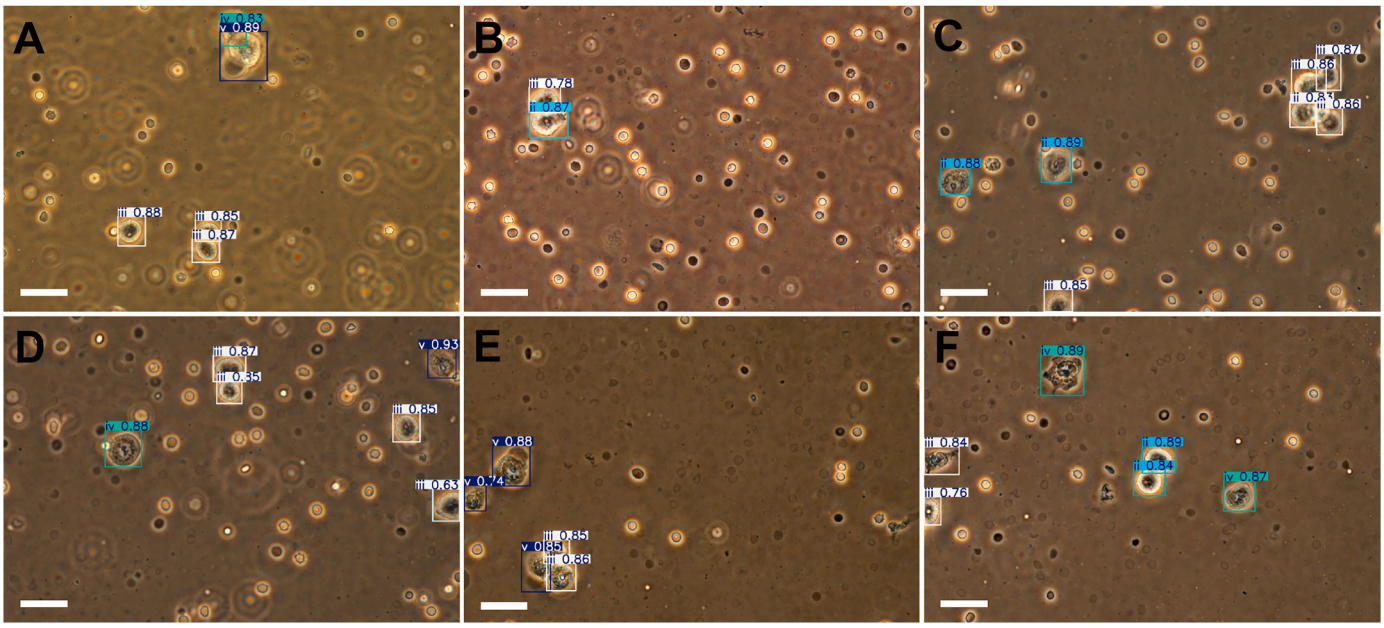


Fig. 3. Deep learning model for invasive capacity quantification of CTC in whole blood samples. Scale bar: 10 μm.

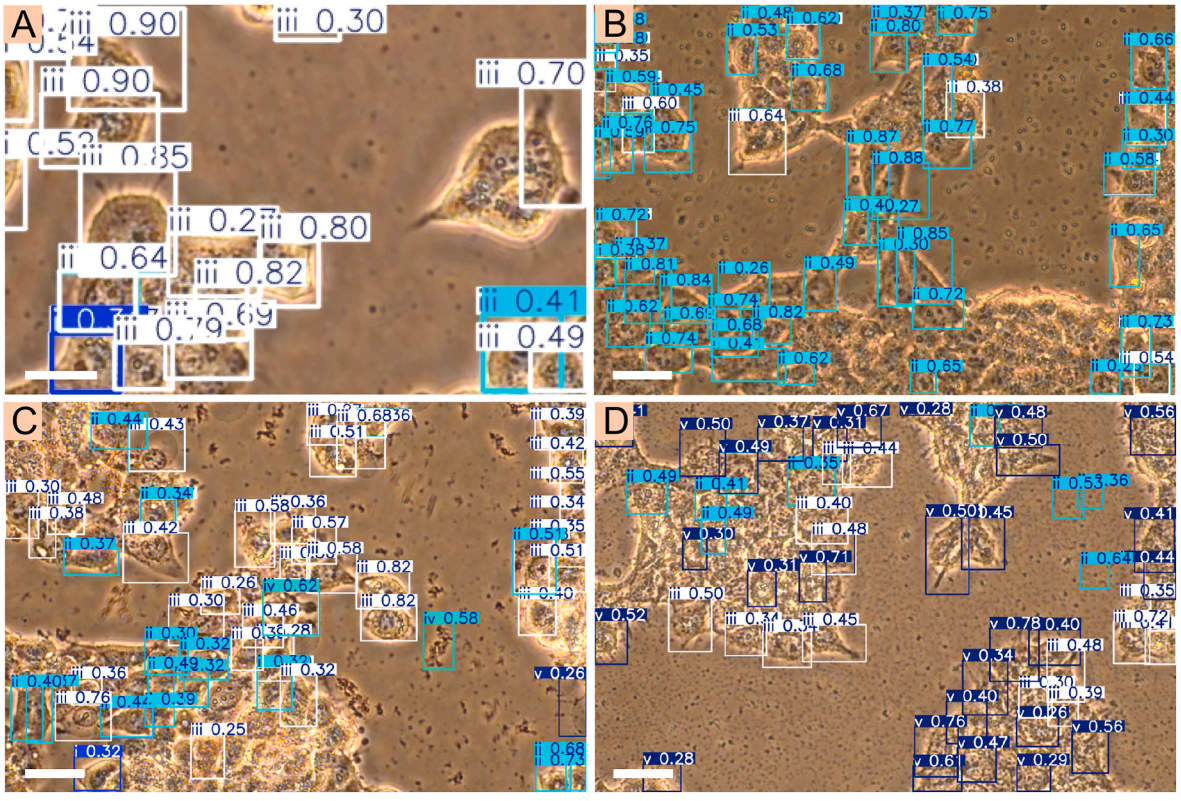


Fig. 4. Deep learning model for drug sensitivity assessment: (A) Cisplatin, (B) Paclitaxel, (C) Doxorubicin, (D) Rapamycin. Scale bar: 10 μm.

truly label-free, non-invasive EMT state evaluation, avoiding the biases and cellular damage associated with labeling. Second, it pioneers the application of an object detection architecture to EMT state analysis, providing simultaneous cell localization, state classification, and invasion capability assessment. Finally, the method maintains high detection sensitivity even within whole blood environments, offering a novel solution for clinical CTC analysis.

Nevertheless, several limitations should be noted. The current model was validated only on the MCF-7 cell line; future studies should include more cell types and primary patient samples. Although we included five EMT states, the process in patient-derived tumors may exhibit greater heterogeneity. Incorporating additional morphological features and temporal information could improve the model's generalizability. Moreover, the current model does not integrate multi-modal data (e.g., gene expression or proteomics), which represents a promising future direction.

Despite these limitations, our method provides a novel label-free analytical tool for cancer metastasis research, demonstrating significant potential for deciphering EMT states in rare CTCs and predicting drug response. Further validation in clinical samples and exploration of its integration with existing molecular biology techniques will be valuable next steps.

4. Conclusion

In this work, we established a deep learning-driven platform for non-invasive, real-time EMT state evaluation in single or rare CTCs using morphological profiling. This method overcomes the limitations of conventional biomarker-dependent techniques by eliminating labeling, minimizing subjectivity, and resolving single-cell heterogeneity. As a universal analytical tool, it holds promise for clinical applications in metastasis prediction, drug sensitivity testing, and adaptive treatment optimization across diverse cancer types.

CRediT authorship contribution statement

Yiyao Yang: Writing – original draft, Formal analysis, Data curation. **Yuxin Guo:** Writing – original draft, Investigation, Data curation. **Zhaoliang Wang:** Supervision, Software, Resources. **Yifan Weng:** Validation. **Tingting Hao:** Project administration. **Qingqing Zhang:** Funding acquisition, Conceptualization. **Shuihua Wang:** Methodology, Funding acquisition, Conceptualization. **Zhiyong Guo:** Writing – review & editing, Supervision, Resources, Funding acquisition, Conceptualization.

Data and code availability

Data are available on request.

Code and raw data relevant to data analysis in this study is available at GitHub (https://github.com/NBUGuozy/EMT) and Zenodo (https://doi.org/10.5281/zenodo.17047914).

Declaration of competing interest

The authors declare that they have no known competing financial interests or personal relationships that could have appeared to influence the work reported in this paper.

Acknowledgements

This work was financially supported by National Natural Science Foundation of China (82273681), Basic Research Program of Jiangsu (BK20241815) and Ningbo Natural Science Foundation (2024J476).

Appendix A. Supplementary data

Supplementary data to this article can be found online at https://doi.org/10.1016/j.bios.2025.118051.

References

Balagopal, A., Nguyen, D., Morgan, H., Weng, Y., Dohopolski, M., Lin, M.H., Barkousaraie, A.S., Gonzalez, Y., Garant, A., Desai, N., Hannan, R., Jiang, S., 2021. Med. Image Anal. 72, 102101. https://doi.org/10.1016/j.media.2021.102101.

Calderaro, J., Ghaffari Laleh, N., Zeng, Q., Maille, P., Favre, L., Pujals, A., Klein, C., Bazille, C., Heij, L.R., Uguen, A., Luedde, T., Di Tommaso, L., Beaufrère, A., Chatain, A., Gastineau, D., Nguyen, C.T., Nguyen-Canh, H., Thi, K.N., Gnemmi, V., Graham, R.P., Charlotte, F., Wendum, D., Vij, M., Allende, D.S., Aucejo, F., Diaz, A., Rivière, B., Herrero, A., Evert, K., Calvisi, D.F., Augustin, J., Leow, W.Q., Leung, H.H. W., Boleslawski, E., Rela, M., François, A., Cha, A.W.H., Forner, A., Reig, M., Allaire, M., Scatton, O., Chatelain, D., Boulagnon-Rombi, C., Sturm, N., Menahem, B., Frouin, E., Tougeron, D., Tournigand, C., Kempf, E., Kim, H., Ningarhari, M., Michalak-Provost, S., Gopal, P., Brustia, R., Vibert, E., Schulze, K., Rüther, D.F., Weidemann, S.A., Rhaiem, R., Pawlotsky, J.M., Zhang, X., Luciani, A., Mulé, S., Laurent, A., Amaddeo, G., Regnault, H., De Martin, E., Sempoux, C., Navale, P., Westerhoff, M., Lo, R.C.L., Bednarsch, J., Gouw, A., Guettier, C., Lequoy, M., Harada, K., Sripongpun, P., Wetwittayaklang, P., Loménie, N., Tantipisit, J., Kaewdech, A., Shen, J., Paradis, V., Caruso, S., Kather, J.N., 2023. Nat. Commun. 14 (1), 8290. https://doi.org/10.1038/s41467-023-43749-3.

Castaneda, M., den Hollander, P., Kuburich, N.A., Rosen, J.M., Mani, S.A., 2022. Semin. Cancer Biol. 87, 17–31. https://doi.org/10.1016/j.semcancer.2022.10.006.

Christiansen, J.J., Rajasekaran, A.K., 2006. Cancer Res. 66 (17), 8319–8326. https://doi.org/10.1158/0008-5472.Can-06-0410.

Courtiol, P., Maussion, C., Moarii, M., Pronier, E., Pilcer, S., Sefta, M., Manceron, P., Toldo, S., Zaslavskiy, M., Le Stang, N., Girard, N., Elemento, O., Nicholson, A.G., Blay, J.Y., Galateau-Sallé, F., Wainrib, G., Clozel, T., 2019. Nat. Med. 25 (10), 1519–1525. https://doi.org/10.1038/s41591-019-0583-3.

Diamantopoulou, Z., Castro-Giner, F., Aceto, N., 2020. J. Exp. Med. 217 (8), e20200356. https://doi.org/10.1084/jem.20200356.

Erin, N., Grahovac, J., Brozovic, A., Efferth, T., 2020. Drug resist. Update 53, 100715. https://doi.org/10.1016/j.drup.2020.100715.

Ertl-Wagner, B., Khalvati, F., 2021. Neuro Oncol. 24 (2), 300–301. https://doi.org/10.1093/neuonc/noab249.

Fang, C., Kang, Y., 2021. Cancer Res. 81 (23), 5800–5802. https://doi.org/10.1158/0008-5472.Can-21-3302.

Gagnon, L., Gupta, D., Mastorakos, G., White, N., Goodwill, V., McDonald, C., Beaumont, T., Conlin, C., Seibert, T., Hattangandi-Gluth, J., Kesari, S., Schulte, J., Piccioni, D., Dale, A., Farid, N., Rudie, J., 2023. Neuro Oncol. 25 (Suppl. ment_5), v191–v192. https://doi.org/10.1093/neuonc/noad179.0726.

Ganesh, K., Massague, J., 2021. Nat. Med. 27 (1), 34–44. https://doi.org/10.1038/s41591-020-01195-4.

Gao, P., Shan, W., Guo, Y., Wang, Y., Sun, R., Cai, J., Li, H., Chan, W.S., Liu, P., Yi, L., Zhang, S., Li, W., Jiang, T., He, K., Wu, Z., 2022. JAMA Netw. Open 5 (8), e2225608. https://doi.org/10.1001/jamanetworkopen.2022.25608.

Gerashchenko, T., Denisov, E., Pautova, D., Zavyalova, M., Cherdyntseva, N., Perelmuter, V., 2016. Ann. Oncol. 27 (Suppl. 6), vi545–vi551. https://doi.org/10.1093/annonc/mdw393.06.

Ida, H., Taira, N., Nashimoto, Y., Kumatani, A., Takahashi, Y., Shiku, H., 2025. Anal. Chem. 97 (1), 312–318. https://doi.org/10.1021/acs.analchem.4c04204.

Jiang, Y., Zhou, K., Sun, Z., Wang, H., Xie, J., Zhang, T., Sang, S., Islam, M.T., Wang, J.Y., Chen, C., Yuan, Q., Xi, S., Li, T., Xu, Y., Xiong, W., Wang, W., Li, G., Li, R., 2023. Cell Rep. Med. 4 (8), 101146. https://doi.org/10.1016/j.xcrm.2023.101146.

Jinesh, G.G., Brohl, A.S., 2022. Signal Transduct. Targeted Ther. 7 (1), 296. https://doi.org/10.1038/s41392-022-01132-6.

Khanbabaei, H., Ebrahimi, S., García-Rodríguez, J.L., Ghasemi, Z., Pourghadamyari, H., Mohammadi, M., Kristensen, L.S., 2022. J. Exp. Clin. Cancer Res. 41 (1), 278. https://doi.org/10.1186/s13046-022-02488-x.

Kiri, S., Ryba, T., 2024. Mol. Cancer 23 (1), 154. https://doi.org/10.1186/s12943-024-02069-w.

Kitz, J., Goodale, D., Postenka, C., Lowes, L.E., Allan, A.L., 2021. Clin. Exp. Metastasis 38 (1), 97–108. https://doi.org/10.1007/s10585-020-10070-y.

Lee, S.H., Jang, H.J., 2022. Clin. Mol. Hepatol. 28 (4), 754–772. https://doi.org/10.3350/cmh.2021.0394.

Li, J., Riedt, T., Goossens, S., Carrillo García, C., Szczepanski, S., Brandes, M., Pieters, T., Dobrosch, L., Gütgemann, I., Farla, N., Radaelli, E., Hulpiau, P., Mallela, N., Fröhlich, H., La Starza, R., Matteucci, C., Chen, T., Brossart, P., Mecucci, C., Huylebroeck, D., Haigh, J.J., Janzen, V., 2017. Blood 129 (4), 460–472. https://doi.org/10.1182/blood-2016-05-714659.

Li, Q., Zhou, Z.W., Duan, W., Qian, C.Y., Wang, S.N., Deng, M.S., Zi, D., Wang, J.M., Mao, C.Y., Song, G., Wang, D., Westover, K.D., Xu, C.X., 2021. J. Exp. Clin. Cancer Res. 40 (1), 220. https://doi.org/10.1186/s13046-021-02006-5.

Li, R., 2023. Nat. Biotechnol. 41, 1521. https://doi.org/10.1038/s41587-023-02038-6.

Lo, H.C., Zhang, X.H.F., 2018. Dev. Cell 45 (6), 663–665. https://doi.org/10.1016/j.devcel.2018.05.033.

Mani, K., Deng, D., Lin, C., Wang, M., Hsu, M.L., Zaorsky, N.G., 2024. Nat. Commun. 15 (1), 1519. https://doi.org/10.1038/s41467-024-45307-x.

Moen, E., Bannon, D., Kudo, T., Graf, W., Covert, M., Van Valen, D., 2019. Nat. Methods 16 (12), 1233–1246. https://doi.org/10.1038/s41592-019-0403-1.

Nakaya, Y., Sheng, G., 2013. Cancer Lett. 341 (1), 9–15. https://doi.org/10.1016/j.canlet.2013.02.037.

Nurmagambetova, A., Mustyatsa, V., Saidova, A., Vorobjev, I., 2023. Sci. Rep. 13, 22164. https://doi.org/10.1038/s41598-023-48279-y.

Pang, A., Carbini, M., Moreira, A.L., Maki, R.G., 2018. J. Clin. Oncol. 36 (2), 210–216. https://doi.org/10.1200/jco.2017.74.9523.

Pastushenko, I., Blanpain, C., 2019. Trends Cell Biol. 29 (3), 212–226. https://doi.org/10.1016/j.tcb.2018.12.001.

Puchinskaya, M., 2019. Ann. Oncol. 30 (Suppl. 7), vii11. https://doi.org/10.1093/annonc/mdz413.040.

Puchinskaya, M., Prokopenia, D., 2020. Ann. Oncol. 31 (Suppl. 4), S252. https://doi.org/10.1016/j.annonc.2020.08.178.

Qian, C.N., Mei, Y., Zhang, J., 2017. Chin. J. Cancer 36, 38. https://doi.org/10.1186/s40880-017-0206-7.

Quinsgaard, E.M.B., Korsnes, M.S., Korsnes, R., Moestue, S.A., 2024. Exp. Cell Res. 437 (1), 113993. https://doi.org/10.1016/j.yexcr.2024.113993.

Saitoh, M., 2023. Semin. Cancer Biol. 97, 21–29. https://doi.org/10.1016/j.semcancer.2023.10.001.

Sandino, A., Verma, R., Chen, Y., Becerra, D., Romero, E., Tiwari, P., 2021. Neuro Oncol. 23 (Suppl. ment_6), vi202–vi203. https://doi.org/10.1093/neuonc/noab196.806.

Savagner, P., 2010. Ann. Oncol. 21, vii89–vii92. https://doi.org/10.1093/annonc/mdq292.

Serrano-Gomez, S.J., Maziveyi, M., Alahari, S.K., 2016. Mol. Cancer 15, 18. https://doi.org/10.1186/s12943-016-0502-x.
Simeonov, K.P., Byrns, C.N., Clark, M.L., Norgard, R.J., Martin, B., Stanger, B.Z., Shendure, J., McKenna, A., Lengner, C.J., 2021. Cancer Cell 39 (8), 1150–1162.e9. https://doi.org/10.1016/j.ccell.2021.05.005.
Singh, M., Yelle, N., Venugopal, C., Singh, S.K., 2018. Pharmacol. Ther. 182, 80–94. https://doi.org/10.1016/j.pharmthera.2017.08.009.
Tian, F., Liu, D., Wei, N., Fu, Q., Sun, L., Liu, W., Sui, X., Tian, K., Nemeth, G., Feng, J., Xu, J., Xiao, L., Han, J., Fu, J., Shi, Y., Yang, Y., Liu, J., Hu, C., Feng, B., Sun, Y., Wang, Y., Yu, G., Kong, D., Wang, M., Li, W., Chen, K., Li, X., 2024. Nat. Med. 30 (5), 1309–1319. https://doi.org/10.1038/s41591-024-02915-w.
Ulianova, E.P., Sagakyants, A.B., Novikova, I.A., Nepomnyashchaya, E.M., Chernikova, E.N., Bakulina, S.M., Pushkareva, T.F., Dzhenkova, E.A., Shaposhnikov, A.V., Kolesnikov, E.N., 2021. J. Clin. Oncol. 39 (15_Suppl. l), e16028. https://doi.org/10.1200/JCO.2021.39.15_suppl.e16028.
Vermeulen, C., Pagès-Gallego, M., Kester, L., Kranendonk, M.E.G., Wesseling, P., Verburg, N., de Witt Hamer, P., Kooi, E.J., Dankmeijer, L., van der Lugt, J., van Baarsen, K., Hoving, E.W., Tops, B.B.J., de Ridder, J., 2023. Nature 622 (7984), 842–849. https://doi.org/10.1038/s41586-023-06615-2.
Whitney, H.M., Li, H., Ji, Y., Liu, P., Giger, M.L., 2020. Proc. IEEE 108 (1), 163–177. https://doi.org/10.1109/JPROC.2019.2950187.
Wu, Z., Lawrence, P.J., Ma, A., Zhu, J., Xu, D., Ma, Q., 2020. Trends Pharmacol. Sci. 41 (12), 1050–1065. https://doi.org/10.1016/j.tips.2020.10.004.
Yang, J., Zhang, X., Zhang, Y., Zhu, D., Zhang, L., Li, Y., Zhu, Y., Li, D., Zhou, J., 2016. J. Exp. Clin. Cancer Res. 35, 26. https://doi.org/10.1186/s13046-016-0298-y.
Zeune, L.L., Boink, Y.E., van Dalum, G., Nanou, A., de Wit, S., Andree, K.C., Swennenhuis, J.F., van Gils, S.A., Terstappen, L.W.M.M., Brune, C., 2020. Nat. Mach. Intell. 2, 124–133. https://doi.org/10.1038/s42256-020-0153-x.
Zhang, Y.E., Stuelten, C.H., 2024. Semin. Cancer Biol. 101, 1–11. https://doi.org/10.1016/j.semcancer.2024.04.001.
Zhao, N., Powell, R.T., Yuan, X., Bae, G., Roarty, K.P., Stossi, F., Strempfl, M., Toneff, M. J., Johnson, H.L., Mani, S.A., Jones, P., Stephan, C.C., Rosen, J.M., 2021. Nat. Commun. 12, 4262. https://doi.org/10.1038/s41467-021-24545-3.